ChemComm

COMMUNICATION

View Article Online
View Journal | View Issue

Cite this: *Chem. Commun.*, 2025, **61**, 12924

Received 13th May 2025,
Accepted 22nd July 2025

DOI: 10.1039/d5cc02717a

rsc.li/chemcomm

Substituents effects on the electrocatalytic CO_2 reduction by cobalt corroles in solution†

Sachin Kumar,[a] Sergio Fernández,[b] Irena Saltsman,[a] Natalia Fridman,[a] Atif Mahammed,[a] Alexander J. M. Miller *[b] and Zeev Gross *[a]

Electrochemical CO_2 reduction catalysis with cobalt corrole complexes in solution is reported. Corroles have attracted attention as contracted and trianionic tetrapyrrolic macrocycles that can be compared to leading porphyrin catalysts for CO_2 reduction, but most studies focus on heterogenized systems with poorly defined electrochemical responses. Electrochemical studies of cobalt corroles bearing axial triphenylphosphine ligands to ensure solubility are reported. The voltammetry provides mechanistic insights supporting CO_2 activation after the formal Co^{II}/Co^{I} reduction. The series of cobalt complexes, including a newly designed corrole with mixed perfluorophenyl/ortho-dimethoxyphenyl substituent pattern, provide evidence for electron-rich catalysts having stronger interactions with CO_2. The primary product of CO_2 reduction is CO, formed at a rate of *ca.* 90 s^{-1}.

The electrocatalytic reduction of CO_2 to energy-dense compounds is currently being pursued as a sustainable approach for manufacturing fuel (sometimes called eFuel).[1,2] Presently, a multitude of catalytic materials are being studied to achieve a shift in the global energy paradigm;[3] and molecular catalysts based on 3d transition metals have attracted interest (in part inspired by analogies to biological energy storage enzymes).[4,5] Metal complexes of porphyrins and phthalocyanines are among the most effective molecular catalysts for CO_2 reduction,[6–8] shown to be capable of catalyzing its transformation into a range of reduced forms, like CO,[4] $HCOO^-$,[9] CH_3OH,[10] and CH_4[11] with high turnover frequencies at moderate overpotentials. There is also increasing activity in employing corroles as metal-chelating ligands for the development of CO_2 reduction catalysts.[12] Corroles act as tri-anionic ligands and supply a coordination core that is about 10% contracted relative to related dianionic tetrapyrrole macrocycles, two factors that can stabilize complexes in high oxidation states while generating complexes that are more reducing or nucleophilic in low oxidation states.[13–15] The first report regarding utilization of cobalt and iron corroles for CO_2 reduction, performed under homogenous conditions (organic solvent, non-modified electrodes) with a comparison to analogous porphyrin complexes,[16] disclosed that electrocatalysis by the former relies on the M^{+1} rather than the M^0 oxidation state.[17] This was followed much later by an investigation deducing small benefits of remote OCH_3 groups present in superstructured derivatives.[17] Most recent reports focused on heterogeneous catalysis (aqueous solutions, catalyst-modified electrodes), performed by depositing cobalt corroles substituted with S-PEG-(7)-OMe anchoring groups on a carbon paper electrode.[12,18] Highly reduced products, such as methanol, ethanol, and acetic acid were observed at relatively low overpotentials at pH 6.[12] High selectivity towards CO production was observed for cobalt corrole catalysts bound to carbon nanotubes and deposited on carbon electrodes.[19,20]

The earlier studies are promising but also raise questions. In solution, only CO has been observed as a carbon-containing product of CO_2 reduction, while on surfaces either CO or highly reduced C_1 and C_2 products are reported. Mechanistic insight has so far been limited, particularly on surfaces where voltammetry is not typically well-defined. And relatively few structural variations have been made, limiting insight into how corrole substituents impact the electrocatalytic performance and alter the reaction mechanism. Studies of well-defined corroles with good solubility can provide important performance comparisons between homogeneous and heterogeneous systems, as well as providing mechanistic insight that is possible with homogeneous molecular catalysis.[21]

The goals of the present study were to deduce how structural and electronic effects of cobalt(III) corrole complexes affect their performance as CO_2 reduction catalysts. Chart 1 shows the catalysts examined. Two known complexes were included: **1a**, with three electron-withdrawing C_6F_5 groups, and the much smaller and more electron-rich **1d**, free of any substituent.[22,23]

[a] *Schulich Faculty of Chemistry, Technion–Israel Institute of Technology, Haifa 320003, Israel. E-mail: chr10zg@technion.ac.il*
[b] *Department of Chemistry, University of North Carolina, Chapel Hill, North Carolina 27599, USA. E-mail: ajmm@email.unc.edu*

† Electronic supplementary information (ESI) available: Characterization like UV-Vis, ^1H NMR, mass and CV Data. CCDC 2421462 and 2421463. For ESI and crystallographic data in CIF or other electronic format see DOI: https://doi.org/10.1039/d5cc02717a

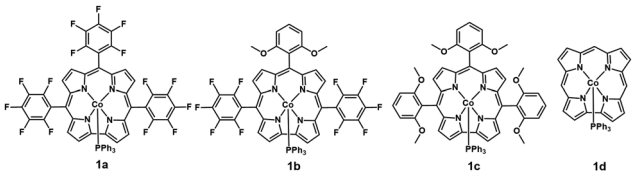

Chart 1 The (triphenylphosphine)cobalt(III) corrole complexes investigated in this work, for deducing the effects of *meso*-substituents on electrocatalytic CO_2 reduction.

Two complexes were newly designed with either one (**1b**) or three (**1c**) 2,6-dimethoxyphenyl groups. The remote OCH_3 moieties might facilitate protons transfer to the active site or stabilize intermediates, while also providing some steric shielding and increasing electron density. Complex **1c** is most electron-rich while **1b** has only one 2,6-dimethoxyphenyl substituent but two C_6F_5 groups whose role is to make the complex easier to reduce.

The new 5-coordinate low-spin d^6 $(PPh_3)Co^{III}$ complexes (**1b**, **1c**) were prepared *via* metallation of their respective free-base corroles,[24–26] and characterized by high resolution mass spectrometry, UV-vis, ^{1}H-NMR, and elemental analysis (Fig. S1–S13, ESI†). Their electronic spectra (Fig. 1a) display characteristic split Soret and Q-bands that are distinct from those of 6-coordinate bis-pyridine cobalt(III) corroles.[27] Axial PPh_3 coordination increases the stability of the pre-catalysts and has been shown to influence the reactivity of cobalt corrole complexes in the catalytic O_2 reduction reactions.[28,29]

X-ray quality crystals were obtained for free-base **1b** (Fig. 1b). Notably, the corrole macrocycle exhibits significant distortion from planarity to reduce steric hindrance between the inner protons. In the resulting structure, the NH protons of rings B and D deviate from the mean plane of the four nitrogen atoms by +0.72 Å and −0.47 Å, respectively, while the NH proton of ring C remains nearly in-plane, with a deviation of only +0.009 Å, while in free base **1a**,[30] these values +0.89 Å and −0.46 Å, and 0.1 Å for ring B. These distortions position the hydrogens at minimal van der Waals distances of 2.07–2.33 Å. Single crystals of complex **1c** were also obtained (by slow evaporation from a DCM/heptane/methanol solvent mixture), enabling a solid-state structure determination (Fig. 1c). Examination of the corresponding data reveals quite large angles between the corrole and the 2,6-dimethoxyphenyl groups (70.3°–80.2°) which brings the remote OCH_3 moieties quite close to the center of the N4 coordination core (Fig. 1c). The cobalt ion is in a square pyramidal geometry placed 0.287 Å above the N_4 plane

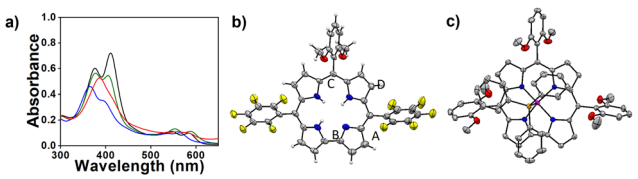

Fig. 1 The (a) electronic spectra (in ethyl acetate) of the (triphenylphosphine)cobalt(III) corroles **1a** (black), **1b** (green), **1c** (blue), and **1d** (red) and ORTEP presentation (pink-cobalt, blue-nitrogen, gray-carbon, red-oxygen, orange-phosphorus) of the X-ray crystal structures obtained for (b) the metal-free corrole of complex **1b** and (c) complex **1c**.

Table 1 Comparison of structural metrics for three of the investigated cobalt corroles

Complex	ΔM_4[a] (Å)	ΔM_{23}[b] (Å)	Co–P (Å)	Co–N[c] (Å)
1a[d]	0.262	0.324	2.210	1.878
1c[e]	0.287	0.381	2.207	1.873
1d[f]	0.278	0.374	2.209	1.872

[a] Deviation of the cobalt ion from the mean plane defined by the 4-core nitrogen atoms. [b] Deviation of the cobalt ion from the mean plane defined by the 23-ring atoms. [c] Average bond length of the cobalt(III) ion with the four equatorial N atoms. [d] Data from ref. 17. [e] Data obtained in this work. [f] Data from ref. 18.

and 0.381 Å from 23 atoms plane (Table 1). The average Co–N bond length is 1.87 Å, and the Co–P distance is 2.207 Å. The through-space distances of the aryl's *ortho*-methoxy O atoms are 5.143 Å to Co, 2.737 Å to the *meso*-C atom, and 4.757 Å to the C atom attached to phosphorus which would be most representative of the oxygen atom in the putative Co–CO_2 adduct. The complex shows high deviation of the cobalt ion from the mean plane defined by the 4-core nitrogen atoms and the 23-core atoms as compared to other cobalt corrole (Table 1).

The four cobalt corroles were studied by cyclic voltammetry (CV) in acetonitrile solution with 0.1 M tetrabutylammonium hexafluorophosphate ($TBAPF_6$) as supporting electrolyte. Each complex displays two reductions, which previous work has suggested are both metal-centered.[22] At a scan rate of 100 mV s^{-1}, all corrole complexes show quasi-reversible or fully irreversible $Co^{III/II}$ features with peak potentials (E_{pc}) of −0.80, −0.93, −1.25 and −0.99 V *vs.* $Fc^{+/0}$ for **1a**, **1b**, **1c** and **1d**, respectively (Fig. 2). The correlation between increased irreversibility and the electron-donating capability of the ligand is attributed to faster and/or more favorable dissociation of the axial PPh_3 ligand upon formation of a d^7 Co^{II} center. Its reoxidation (E_{pa}) hence takes places either on the 5-coordinate PPh_3-bound complex (small peak-to-peak separation) or on the 4-coordinate PPh_3-free Co^{II} corrole (large peak-to-peak separation).[28] Both processes apparently occur for **1b** and **1d**, while for the most electron-poor and hence most Lewis acid **1a** the PPh_3 remains mostly bound and for **1c** the PPh_3 is completely dissociated upon reduction. Varying the scan rate of the CV of **1c** reveals an anodic shift of the $Co^{III/II}$ irreversible wave at slower scan rates, consistent with ligand dissociation after reduction (Fig. S14 (ESI†). More reducing potentials lead to reversible features at −1.82, −1.96, −2.20 and −2.12 V *vs.* $Fc^{+/0}$ which have been assigned to the formal $Co^{II/I}$ redox couples of **1a**, **1b**, **1c** and **1d**, respectively. On top of affecting the Lewis acidity, the substituents on the *meso*-carbon induce a monotonic electrochemical response within the examined series.[31] Both the $Co^{III/II}$ and $Co^{II/I}$ processes appear more negative as the electron-donating character of the ligand is increased. Focusing on the reversible $Co^{II/I}$ process, this translates into a 360 mV more positive $E_{1/2}$ in the case of **1a** compared to **1c** (three C_6F_5 *vs.* 2,6-dimethoxyphenyl groups) and the same process for **1c** is 60 mV more negative relative to **1d**. The dianionic 4-coordinate d^8 cobalt(I) corroles with two electrons in the high energy d_z^2 orbital may be anticipated to have a high affinity towards electrophiles in general and carbon dioxide in particular.[12]

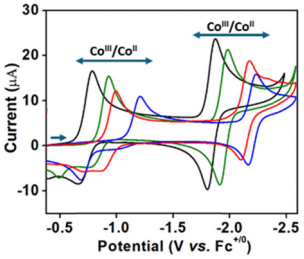

Fig. 2 Cyclic voltammograms (100 mV s^{-1}) of the Co corrole complexes (1 mM) **1a** (black), **1b** (green), **1c** (blue), and **1d** (red) in anhydrous MeCN/$TBAPF_6$, 0.1 M electrolyte solution under N_2 atmosphere.

Examination of the CVs of the complexes in MeCN containing 1% H_2O under a nitrogen atmosphere uncovered that both the first and second reduction waves were unaffected (Fig. 3, red traces). This observation suggests that the electrochemically generated Co^{II} and Co^{I} species are not sufficiently reactive toward proton reduction, *i.e.* that they not catalyze the hydrogen evolution reaction (HER) under these conditions. In contrast, when the atmosphere was switched from N_2 to CO_2 in the presence of 1% H_2O the second reduction wave-corresponding to the $Co^{II/I}$ redox couple-became irreversible with a notable increase in current (Fig. 3, blue traces). This implies a strong interaction between the electrochemically generated Co^{I} species and CO_2, likely resulting in the formation of $[Co–CO_2]^{2-}$ or $[Co–CO_2H]^{-}$ adducts. The complexes bearing electron-withdrawing C_6F_5 substituents (**1a** and **1b**) did not exhibit an anodic shift in the $Co^{II/I}$ couple when moving from N_2 to CO_2 atmosphere, suggesting quite a weak interaction with CO_2. In contrast, the much more electron-rich complexes (**1c** and **1d**) displayed pronounced anodic shifts (Fig. 3c and d), consistent with enhanced rate constants for CO_2 binding due to high nucleophilicity of metal centre.

Following the indications regarding CO_2 binding to the cobalt(I) corroles, an increase in current consistent with electrocatalysis was observed at potentials slightly more negative than the $Co^{II/I}$ redox couple. These were also much better defined and most pronounced for **1c** and **1d**, with the latter reaching current densities of up to 2.05 mA cm^{-2} (Fig. 3, blue traces). Full analysis of catalysis by **1d** is difficult since the curve crossing observed in its CV suggests a side reaction. But catalyst **1c** has a well-defined voltammogram that includes a plateau shape, which enables a rate analysis to determine the observed rate constant for the turnover-limiting catalytic step (k_{obs}), which is equivalent to the turnover frequency under these conditions (TOF_{max}). Based on the ratio of the catalytic current (i_c) to the current of the second reduction (i_p) at scan rates where i_c/i_p becomes nearly constant, the rate constant for the catalytic process was estimated as k_{obs} = 90 s^{-1} (Fig. S16, S17 and Table S2, ESI†). It is likely that **1d** has similar or even larger activity, but its voltammogram did not meet the criteria for quantitative analysis. This set of observations is in line with previous reports where Co^{I} was identified as the active species for CO_2 binding, leading to electrocatalytic CO_2 reduction.

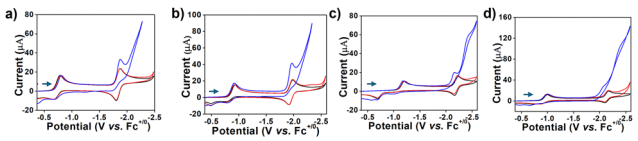

Fig. 3 Cyclic voltammograms recorded for (a) **1a**, (b) **1b**, (c) **1c** and (d) **1d** dissolved in anhydrous CH_3CN under N_2, 1% H_2O under N_2, and 1% H_2O under CO_2 (the black, red and blue traces, respectively).

These investigations were followed by identifying and characterizing the gaseous products obtained by performing controlled potential electrolysis (CPE, Fig. S18, ESI†) over 20 minutes with all the catalysts in the series in CH_3CN solution containing 1 mM catalyst and 1% H_2O under CO_2 atmosphere. The results summarized in Table 2 show that almost no products were obtained *via* catalysis by **1a**, while for the other three catalysts CO gas was the major product, accompanied by a very small amount of H_2. Similar performance was observed for catalysts **1b** and **1c**. The latter aspect is fully consistent with the earlier described indications (the red traces in Fig. 3), which is important since CO_2 reduction catalysis is very often hampered by HER activity.[32] Increasing the H_2O content to 10% or adding phenol (50 mM) as a stronger acid did not improve the CO_2 reduction selectivity to CO for **1c** (Table S4, ESI†). That **1a** is the most sluggish catalyst is also in accord with the rather small catalytic waves seen in Fig. 3a, which suggests that while having electron-withdrawing *meso*-C substituents is beneficial for accessing the cobalt(I) state at less negative potentials that also decreases its reactivity regarding CO_2 activation. Comparison of the three much more electron-rich complexes suggests that the hanging OCH_3 moieties present in catalysts **1b** and **1c** are not advantageous, at least under the conditions of limited amounts of a weak proton donor like water. In fact, complex **1d** with no *meso*-C substituents provided somewhat better results in terms of both faradaic efficacy (FE) and diminished HER activity. A rinse test was performed with the best-behaved catalyst **1c**, with the electrode surface rinsed well with solvent after an electrolysis before a second CPE was conducted in electrolyte containing no dissolved catalyst. Almost no current passed in the second electrolysis (Fig. S19, ESI†), suggesting that no active heterogeneous catalyst was deposited onto the surface during CPE.

In summary, we have investigated electrochemical CO_2 reduction by Co^{III} corrole complexes that differ significantly in terms of the *meso*-C substituents: electron-withdrawing C_6F_5 substituents only, combinations of those and electron-donating 2,6-dimethoxyphenyl groups, and no substituents. None of the

Table 2 Results after 20 min CPE under CO_2 with 1% H_2O in MeCN $TBAPF_6$ electrolyte. E_{CPE} is the applied potential in V *vs.* $Fc^{+/0}$

Cat	$E_{1/2}$ *vs.* $Fc^{+/0}$	E_{CPE} (V)	FE_{CO}[a] (%)	FE_{H_2}[a] (%)
1a[b]	−1.86	−2.2	<1	<1
1b	−1.96	−2.2	31	2
1c	−2.20	−2.4	33	1
1d	−2.12	−2.4	37	<1

[a] The faradaic efficiency values for CO and H_2 (FE_{CO} and FE_{H_2}) are based on headspace analysis. [b] Performing CPE for 150 min provides 11% CO and 2% H_2.

complexes efficiently catalyzed hydrogen evolution under homogenous conditions with 1% H_2O as proton source, but all the three electron-rich complexes facilitated electrocatalytic CO_2 reduction to CO with moderate FE. The studies here uncover the importance of delicate tuning of redox potentials for achieving good catalytic activity and introduce one new catalyst that proved to be the best-defined for rate analysis and provide insight into the mechanism of CO_2 reduction with soluble corroles.

It is noteworthy that no highly reduced products were detected, whereas products including methanol, ethanol, and acetic acid have been observed in heterogenized corroles in low to moderate faradaic efficiency.[12,18–20] The conditions are slightly different between those reports and the present study, with fully aqueous conditions possible with heterogeneous catalysis while mixed acetonitrile/water was used here to ensure homogeneous conditions. Specific interactions with the support materials may also give rise to changes in electronic structure, as proposed for Co phthalocyanine catalysts.[33] While further studies are needed to fully elucidate differences in homogeneous *vs.* heterogeneous CO_2 reduction with corroles, this work again shows that the product distribution can differ significantly between the systems. Whereas experimental analysis of individual reaction steps is difficult in the heterogeneous catalysts, the homogeneous system described here enabled insight into the ligand dissociation and CO_2 binding steps in the mechanism of this emerging class of CO_2 reduction electrocatalysts.

This research was supported by the grants from the Israel Ministry of Innovation Science and Technology (MOST) and from the Israel Council for Higher Education-VATAT (grant #1024460). Electrochemical studies were supported by the Center for Hybrid Approaches in Solar Energy to Liquid Fuels (CHASE), an Energy Innovation Hub funded by the U.S. Department of Energy, Office of Science, Office of Basic Energy Sciences under Award Number DE-SC0021173. Some NMR spectroscopy work was conducted in the University of North Carolina's Department of Chemistry NMR Core Laboratory, supported by the U.S. National Science Foundation under grant no. CHE-1828183. S. F. acknowledges the Ramón Areces Foundation for a postdoctoral research fellowship.

Conflicts of interest

There are no conflicts to declare.

Data availability

The data supporting this article have been included as part of the ESI.†

Notes and references

1 S. Ren, D. Joulié, D. Salvatore, K. Torbensen, M. Wang, M. Robert and C. P. Berlinguette, *Science*, 2019, **365**, 367–369.
2 X. Zhang, J. Li, Y. Y. Li, Y. Jung, Y. Kuang, G. Zhu, Y. Liang and H. Dai, *J. Am. Chem. Soc.*, 2021, **143**, 3245–3255.
3 D. Gao, H. Zhou, F. Cai, D. Wang, Y. Hu, B. Jiang, W. Bin Cai, X. Chen, R. Si, F. Yang, S. Miao, J. Wang, G. Wang and X. Bao, *Nano Res.*, 2017, **10**, 2181–2191.
4 J. M. S. Cyrille Costentin, S. Drouet and M. Robert, *Science*, 2012, **338**, 90–94.
5 J. Zheng, D. Zhou, J. Han, J. Liu, R. Cao, H. Lei, H. Bian and Y. Fang, *J. Phys. Chem. Lett.*, 2022, **13**, 11811–11817.
6 S. Amanullah, P. Saha, A. Nayek, M. E. Ahmed and A. Dey, *Chem. Soc. Rev.*, 2021, **50**, 3755–3823.
7 Z. Yin, M. Zhang, Y. Long, H. Lei, X. Li, X.-P. Zhang, W. Zhang, U.-P. Apfel and R. Cao, *Angew. Chem., Int. Ed.*, 2025, **64**, e202500154.
8 P. Saha, S. Amanullah and A. Dey, *Acc. Chem. Res.*, 2022, **55**, 134–144.
9 C. G. Margarit, N. G. Asimow, C. Costentin and D. G. Nocera, *ACS Energy Lett.*, 2020, **5**, 72–78.
10 C. Zhang, J. Follana-Berná, D. Dragoe, Z. Halime, P. Gotico, Á. Sastre-Santos and A. Aukauloo, *Angew. Chem., Int. Ed.*, 2024, **63**, e202411967.
11 S. Patra, S. Bhunia, S. Ghosh and A. Dey, *ACS Catal.*, 2024, **14**, 7299–7307.
12 S. Gonglach, S. Paul, M. Haas, F. Pillwein, S. S. Sreejith, S. Barman, R. De, S. Müllegger, P. Gerschel, U. P. Apfel, H. Coskun, A. Aljabour, P. Stadler, W. Schöfberger and S. Roy, *Nat. Commun.*, 2019, **10**, 1–10.
13 Z. Gross and H. Gray, *Comments Inorg. Chem.*, 2006, **27**, 61–72.
14 C. D. Natale, C. P. Gros and R. Paolesse, *Chem. Soc. Rev.*, 2022, **51**, 1277–1335.
15 A. Mahammed, H. Gray and Z. Gross, *Chem. Rev.*, 2025, **125**, 2809–2845.
16 J. Grodkowski, P. Neta, E. Fujita, A. Mahammed, L. Simkhovich and Z. Gross, *J. Phys. Chem. A*, 2002, **106**, 4772–4778.
17 W. Sinha, A. Mahammed, N. Fridman, Y. Diskin-Posner, L. J. W. Shimon and Z. Gross, *Chem. Commun.*, 2019, **55**, 11912–11915.
18 R. De, S. Gonglach, S. Paul, M. Haas, S. S. Sreejith, P. Gerschel, U.-P. Apfel, T. H. Vuong, J. Rabeah, S. Roy and W. Schöfberger, *Angew. Chem., Int. Ed.*, 2020, **59**, 10527–10534.
19 C. Zhang, P. G. Julliard, D. Dragoe, A. Aukauloo and G. Canard, *Eur. J. Inorg. Chem.*, 2024, 202400318.
20 A. Zamader, A. Singh, B. Giri, M. Caruso, W. R. Osterloh, N. Desbois, C. P. Gros and M. Robert, *ACS Catal.*, 2025, **15**, 11093–11102.
21 F. Franco, C. Rettenmaier, H. S. Jeon and B. Roldan Cuenya, *Chem. Soc. Rev.*, 2020, **49**, 6884–6946.
22 L. Simkhovich, N. Galili, I. Saltsman, I. Goldberg and Z. Gross, *Inorg. Chem.*, 2000, **39**, 2704–2705.
23 A. Kumar, P. Yadav, M. Majdoub, I. Saltsman, N. Fridman, S. Kumar, A. Kumar, A. Mahammed and Z. Gross, *Angew. Chem., Int. Ed.*, 2021, **60**, 25097–25103.
24 B. Koszarna and D. T. Gryko, *J. Org. Chem.*, 2006, **71**, 3707–3717.
25 F. Mandoj, S. Nardis, G. Pomarico, M. Stefanelli, L. Schiaffino, G. Ercolani, L. Prodi, D. Genovese, N. Zaccheroni, F. R. Fronczek, K. M. Smith, X. Xiao, J. Shen, K. M. Kadish and R. Paolesse, *Inorg. Chem.*, 2009, **48**, 10346–10357.
26 I. Yadav and M. Shankar, *Inorg. Chem.*, 2023, **62**, 19956–19970.
27 A. Kumar, S. Fite, A. Raslin, S. Kumar, A. Mizrahi, A. Mahammed and Z. Gross, *ACS Catal.*, 2023, **13**, 13344–13353.
28 A. Raslin, J. C. Douglin, A. Kumar, M. Fernandez-Dela-Mora, D. R. Dekel and Z. Gross, *Inorg. Chem.*, 2023, **62**, 14147–14151.
29 R. Paolesse, L. Jaquinod, D. J. Nurco, S. Mini, F. Sagone, T. Boschi and K. M. Smith, *Chem. Commun.*, 1999, 1307–1308.
30 Z. Gross, N. Galili, L. Simkhovich, I. Saltsman, M. Botoshansky, D. Blaser, R. Boese and I. Goldberg, *Org. Lett.*, 1999, **4**, 599–602.
31 A. Kumar, S. Fite, A. Raslin, S. Kumar, A. Mizrahi, A. Mahammed and Z. Gross, *ACS Catal.*, 2023, **13**, 13344–13353.
32 A. Ogawa, K. Oohora and T. Hayashi, *Inorg. Chem.*, 2018, **57**, 14644–14652.
33 J. Su, C. B. Musgrave III, Y. Song, L. Huang, Y. Liu, G. Li, Y. Xin, P. Xiong, M. M.-J. Li, H. Wu, M. Zhu, H. M. Chen, J. Zhang, H. Shen, B. Z. Tang, M. Robert, W. Goddard and R. Ye, *Nat. Catal.*, 2023, **15**, 818–828.